

Understanding the Light-Intensity Dependence of the Short-Circuit Current of Organic Solar Cells

Paula Hartnagel and Thomas Kirchartz*

In organic solar cells, bimolecular recombination is a key factor limiting the device performance and creating the need for characterization.

Light-intensity-dependent short-circuit current density measurements are a frequently used tool to qualitatively analyze bimolecular recombination in a device. When applying a 0D model, bimolecular recombination is expected to reduce the otherwise linear correlation of the short-circuit current density J_{sc} and the light intensity Φ to a sublinear trend. It is shown by numerical simulations that the slope of the J_{sc} – Φ curve is affected by the recombination mechanism (direct or via traps), the spatial distribution of charge carriers and—in thick solar cells—by space charge effects. Only the combination of these effects allows proper explanation of the different cases, some of which cannot be explained in a simple 0D device model.

1. Introduction

Recent progress in the design of novel donor and non-fullerene acceptor materials has led to substantial progress in organic solar cell efficiencies and stability in the last years.^[1–11] Most of the high efficiency solar cells reported recently feature higher short-circuit current densities^[2] and open-circuit voltages^[12,13] than previously achieved with fullerene based devices of similar bandgaps. At high absorber thicknesses of around 300 nm, however, the current generation of organic solar cells still suffers from at most decent fill factors suggesting problems with charge collection.^[6,14–16] Thus, characterization of

recombination and transport as the two key factors limiting charge collection remains an important research topic.


Nonradiative recombination in organic solar cells is often bimolecular, i.e., the recombination rate scales linearly with the product of electron and hole concentrations. This process is a peculiar feature of organic solar cells that is due to the rather large energies of vibrational modes in organic semiconductors that allow bimolecular nonradiative recombination.^[17–20] For inorganic semiconductors with their lower phonon energies, defects are necessary to allow efficient multiphonon^[21–26] recombination which is then however not bimolecular but linear in the density of minority carriers. Thus, recombination in organic solar

cells is mostly nonlinear in charge-carrier density^[27,28] and therefore—depending on the working point—also in light intensity. Due probably to its simplicity, the linearity of the short-circuit current density J_{sc} is among the most frequently used assays of bimolecular recombination in the field of organic photovoltaics.^[29–37] The interpretation of the light-intensity dependence of J_{sc} in terms of bimolecular recombination is based on the idea that one photon creates one electron and one hole, i.e., both concentrations n (for electrons) and p (for holes) should scale linearly with light intensity. If there is a recombination term that is proportional to the product np , recombination should scale quadratically with light intensity. Thus, if recombination at short circuit is negligible, the short-circuit current density should be proportional to light intensity. If, however, bimolecular recombination reduces the number of collected electrons and holes it should be visible by a sublinear increase in J_{sc} . This rationale is based on a strictly 0D model. All spatial dependences of n and p or the recombination rate $R \sim np$ are ignored in the above line of arguments. This neglect of spatial dependences is not a higher order effect that might be important for a quantitative analysis of the data but it is the reason that the rationale discussed above is wrong in a wide range of situations. One can both observe a linear J_{sc} – Φ relation despite the presence of bimolecular recombination but also a nonlinear J_{sc} – Φ relation for a cell that is dominated by defect assisted recombination that is typically considered to be monomolecular. While it has been discussed before^[38] that substantial amounts of bimolecular recombination are compatible with highly linear J_{sc} – Φ relations; a thorough theoretical discussion of the different effects needed to interpret the light-intensity dependence of J_{sc} is currently missing.

Here, we explain the impact of bimolecular and monomolecular recombination on the J_{sc} in a thin device and in a solar cell

P. Hartnagel
IEK5-Photovoltaik
Forschungszentrum Jülich
Jülich 52425, Germany
Prof. T. Kirchartz
IEK5-Photovoltaik
Forschungszentrum Jülich
Jülich 52425, Germany
E-mail: t.kirchartz@fz-juelich.de

Prof. T. Kirchartz
Faculty of Engineering and CENIDE
University of Duisburg-Essen
Carl-Benz-Str. 199 Duisburg 47057, Germany

 The ORCID identification number(s) for the author(s) of this article can be found under <https://doi.org/10.1002/adts.202000116>

© 2020 The Authors. Published by Wiley-VCH GmbH. This is an open access article under the terms of the Creative Commons Attribution License, which permits use, distribution and reproduction in any medium, provided the original work is properly cited.

DOI: 10.1002/adts.202000116

with high active layer thickness with simulations studying the spatial distribution of charge carriers and their recombination. First, we define the recombination mechanisms implemented in our simulations alongside the theory of how they are supposed to be identified from light-intensity-dependent J_{sc} -measurements. Second, we explain space charges and introduce their possible impact on the photocurrent. Then we present our simulation results on thin devices, where the generation rate is constant throughout the active layer and space-charge effects are small. We discuss that not only bimolecular recombination can cause a nonlinear J_{sc} - Φ relation but also trap-assisted recombination due to the changing of the density of trapped charge carriers with light intensity. As organic solar cells with thick active layers are of special interest for commercialization,^[39–43] we also show simulations of thick devices and highlight the origin and the impact of space charges that evoke a sublinear J_{sc} - Φ relation.^[29,44,45] This detailed discussion on the light-intensity dependence of the J_{sc} allows us to better understand the information on recombination mechanisms in a solar cell that can be extracted from the corresponding measurements.

2. Theory

The most frequently used analysis of light-intensity-dependent short-circuit current density measurements is based on a 0D model of the short-circuit current density J_{sc} . When there is no recombination occurring inside a solar cell at short circuit, all charge carriers generated are also extracted by the electric field. Therefore, the maximum short-circuit current density $J_{sc,max}$ can be written as

$$J_{sc,max} = q \int_0^d G(x) dx = qd\bar{G} \quad (1)$$

where q is the elementary charge and d is the thickness of the absorber. The average generation rate \bar{G} is defined as arithmetic mean of the generation rate G over the position x in the active layer, creating a linear correlation between $J_{sc,max}$ and the generation rate and therefore the illumination. This maximum short-circuit current density is reduced by recombination of free charge carriers. Nongeminate, monomolecular recombination is one possible recombination mechanisms. It describes the recombination of one free charge carrier with another charge carrier that is trapped in a defect state within the energy gap. These deep defects states have been found in various types of organic solar cells originating from the energetic disorder of the materials and depending on factors like thermal annealing and prolonged illumination.^[46–49] The recombination via these defects can be quantified by Shockley–Read–Hall recombination statistics. For trap states in the center of the bandgap, the recombination rate R_{SRH} is given by

$$R_{SRH}(x, \Phi) = \frac{n(x, \Phi) p(x, \Phi)}{\tau_p n(x, \Phi) + \tau_n p(x, \Phi)} \quad (2)$$

Here, n is the electron concentration, p is the hole concentration and $\tau_{n/p}$ is the charge-carrier lifetime. By assuming $\tau_n = \tau_p$ and by using the 0D approximation, the recombination-current density $J_{rec,SRH}$ can be written as

$$J_{rec,SRH}(\Phi) = q \int_0^d R_{SRH}(x, \Phi) dx \approx qd\bar{R}_{SRH}(\Phi) \approx qd\frac{\bar{n}(\Phi)}{2\tau_n} \quad (3)$$

with the average recombination rate \bar{R}_{SRH} via deep traps and the average charge-carrier density \bar{n} . The charge-carrier density is assumed to scale linearly with the generation rate. Hence, the recombination-current density results in

$$J_{rec,SRH}(\bar{G}) = f_1 \bar{G} \quad (4)$$

where f_1 is a coefficient determining the intensity of the monomolecular recombination.

Bimolecular recombination is often assumed to be the dominant recombination mechanism in organic solar cells.^[50–52] This process occurs nonradiatively where a free electron and a free hole recombine with each other. As both types of free charge carriers contribute to this direct recombination process, the direct recombination rate R_{dir} is given by

$$R_{dir}(x, \Phi) = k_{dir} n(x, \Phi) p(x, \Phi) \quad (5)$$

with the direct recombination coefficient k_{dir} . When neglecting all spatial dependences, the recombination-current density $J_{rec,dir}$ by direct recombination can be approximated by

$$J_{rec,dir}(\Phi) = q \int_0^d R_{dir}(x, \Phi) dx \approx qdk_{dir} \bar{n}(\Phi) \bar{p}(\Phi) \quad (6)$$

In case of the average electron density \bar{n} and the average hole density \bar{p} scaling linearly with the generation rate, $J_{rec,dir}$ can be written as

$$J_{rec,dir}(\bar{G}) = f_2 \bar{G}^2 \quad (7)$$

where f_2 is a coefficient indicating the amount of direct recombination.

In a solar cell with both mono- and bimolecular recombination, the recombination-current densities diminish the optimum short-circuit current density to the actual short-circuit current density

$$J_{sc}(\bar{G}) = qd\bar{G} - f_1 \bar{G} - f_2 \bar{G}^2 \quad (8)$$

With this approach, an expression for J_{sc} is acquired linking it to the average generation rate. Both the maximum short-circuit current density and the monomolecular recombination-current density scale linearly with the generation rate whereas bimolecular recombination scales in quadratic order. For better visualization, we calculate the slope

$$\gamma = \frac{d \ln(J_{sc})}{d \ln(\bar{G})} = 1 + \frac{d \ln(1 - f_1 - f_2 \bar{G})}{d \ln(\bar{G})} \quad (9)$$

of the double-logarithmic plot which represents the correlation between J_{sc} and \bar{G} . It appears that in case of no bimolecular, direct recombination ($f_2 = 0$), $\gamma = 1$ and J_{sc} scales linearly with the generation rate. In the presence of direct recombination ($f_2 > 0$); however, a sublinear trend can be observed. Thereby, the measurement of the short-circuit current density for different light

intensities and therefore different generation rates promises an easy way of identifying bimolecular recombination in an organic solar cell from a sublinear relation. However, it requires neglecting the spatial dependence of the generation and the recombination rate. Also, the method only considers recombination via deep traps and direct recombination, but not recombination with charge carriers trapped in energetic states close to the highest occupied molecular orbital (HOMO) or lowest unoccupied molecular orbital (LUMO) level. The density of states of these exponential band tails resulting from the energetic disorder of the organic semiconductor is characterized by the Urbach energy E_U . Typical values for E_U in organic solar cells can be found between 30 and 80 meV.^[48,53–55] Recently, the development of materials with low Urbach energies have enabled organic solar cells with efficiencies above 16%.^[7,56] These findings have highlighted the importance of tail state recombination on the solar cell performance. Therefore, it is essential to understand the impact of substantial amounts of tail states on typically used characterization methods such as the light-intensity dependence of the short-circuit current density.

These defect states in the energy gap can be a source for space charge.^[55,57] When capturing an electron, an acceptor-like defect is negatively charged. This density n_T of trapped electrons is also accounted in the total charge density $\rho = q(p - n - n_T)$. Vice versa, a donor-like defect is a spatially localized positive charge when it is occupied by a hole. Consequently, the trapped hole density p_T changes the total charge density $\rho = q(p - n + p_T)$. According to Poisson's equation

$$\Delta\varphi = -\nabla \cdot \vec{E} = -\frac{\rho}{\epsilon_0\epsilon_r} \quad (10)$$

where φ is the electrostatic potential, \vec{E} the electric field, ϵ_0 the dielectric constant, and ϵ_r the relative permittivity, this spatial increase in carrier density causes a change in electric field. Therefore, the presence of space charge is correlated with a high change of the electric field in the space-charge region. To identify the effect of space charge in simulations, one can set an infinitely high relative permittivity causing a constant electric field. In a sufficiently thin active layer, the width of this space-charge region is equal to the layer thickness and no effect can be observed. However, when the layer thickness is exceeding the width of the space-charge region, a nonconstant electric field occurs. Within the space-charge region, the accumulated charge carriers, e.g., holes, have the drift length $L_{\text{drift}} = \mu_h \tau_h E$, where μ_h is the hole mobility and τ_h the hole lifetime. The electric field $E = \Delta\varphi/w_{\text{SCR}}$ can be approximated by the drop $\Delta\varphi$ of electrostatic potential and the width w_{SCR} of the space-charge region. When assuming $L_{\text{drift}} = w_{\text{SCR}}$,^[44,45] the photocurrent in the space-charge region is given by^[44]

$$J_{\text{ph}} = qGw_{\text{SCR}} = qG(\mu_h \tau_h)^{1/2} \Delta\varphi^{1/2} \quad (11)$$

For a strong accumulation of charges, the space-charge limited current density J_{SCL} is described by^[58]

$$J_{\text{SCL}} = \frac{9}{8} \epsilon_0 \epsilon_r \mu_h \frac{\Delta\varphi^2}{w_{\text{SCR}}^3} \quad (12)$$

and was first derived for a unipolar device by Mott and Gurney, but was later applied to diodes as well.^[44,45] When $J_{\text{ph}} = J_{\text{SCL}}$, the width of the space-charge region can be written as^[45]

$$w_{\text{SCR}} = (9\epsilon_0\epsilon_r\mu_h/8qG)^{1/4} \Delta\varphi^{1/2} \quad (13)$$

Inserting this expression into Equation (11), we obtain the maximum photocurrent in a space-charge limited device^[44]

$$J_{\text{ph}} = q \left(\frac{9\epsilon_0\epsilon_r\mu_h}{8q} \right)^{1/4} G^{3/4} \Delta\varphi^{1/2} \quad (14)$$

It is notable that in this case the photocurrent scales with $G^{3/4}$. This dependence has also been found by Wilken et al. who additionally considered the spatial dependence of the electron and hole current.^[59] The correlation has already been used in previous studies to identify space-charge limited photocurrent in organic solar cells with asymmetric carrier mobilities.^[30,45] However, Equation (12) is only valid in a defect free device with sharp band edges.^[60] For tail states in a unipolar device, the Mark–Helfrich equation describes the space-charge limited current density

$$J_{\text{SCL,MH}} = q^{1-l} \mu_h N_v \left(\frac{\epsilon_0 \epsilon_r l}{N_t (l+1)} \right)^l \left(\frac{2l+1}{l+1} \right)^{l+1} \frac{\Delta\varphi^{l+1}}{w_{\text{SCR}}^{2l+1}} \quad (15)$$

with the density of states N_v in the valence band, the trap density N_t and $l = E_U/k_B T$, where $k_B T$ is the thermal energy.^[61] Since Equation (15) neglects diffusion currents,^[60,62] it is rather a qualitative description than a precise analytical expression for the space-charge limited current. To the best of our knowledge, the Mark–Helfrich equation has not yet been applied to a bipolar device (i.e., a solar cell), though. Therefore, in order to study the light-intensity dependence of the photocurrent in a solar cell, we follow the derivation for the defect-free case using Equation (15) for a diode with tail states. Thereby, we get

$$J_{\text{ph,MH}} \propto G^{1-1/(2l+2)} \quad (16)$$

with the slope

$$\gamma_{\text{MH}} = \frac{d \ln(J_{\text{ph,MH}})}{d \ln(G)} = 1 - \frac{1}{2(E_U/k_B T + 1)} \quad (17)$$

indicating a sublinear increase of the photocurrent with illumination depending on the Urbach energy E_U . When E_U approaches the thermal energy, Equation (17) yields the same light-intensity dependence as the defect-free case in Equation (14). According to Equation (17), wider Urbach tails should feature a light-intensity dependence of the photocurrent closer to linearity than tails with small values of E_U ; a result which appears counterintuitive at first. Both this relation and the more commonly used approach to calculate the space-charge limited photocurrent without trap states demonstrate that a sublinear correlation of the short-circuit current density J_{sc} and the illumination Φ can be expected in organic solar cells with and without defect states. These space-charge effects that require a spatially resolved analysis of the processes inside a solar cell are also not considered in the 0D model from Equation (9).

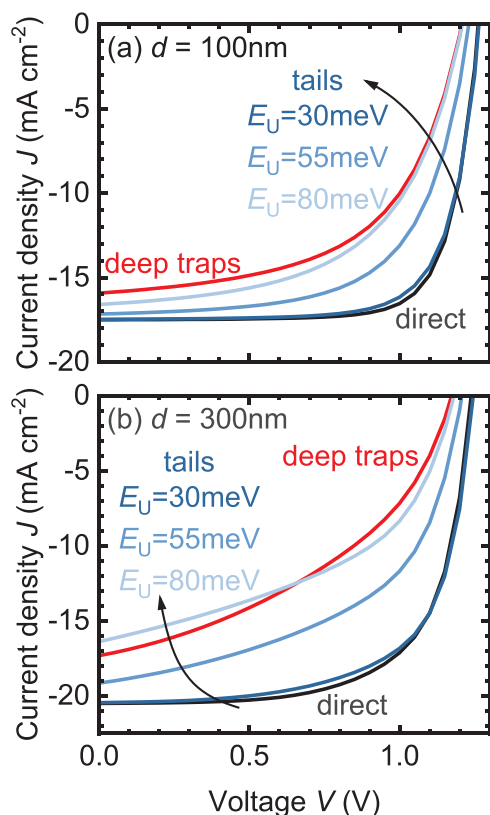


Figure 1. a) Current-density–voltage characteristics of the solar cells modeled with an active layer thickness $d = 100$ nm and constant generation throughout the solar cell under 1 sun illumination. Each simulation contains only one recombination mechanism, namely direct recombination, tail state recombination with three different Urbach energies E_U or recombination via deep traps. b) Characteristics for a higher absorber thickness $d = 300$ nm with spatial dependence of the generation rate. The recombination parameters were chosen to create a decreasing power conversion efficiency from direct recombination to trap-assisted recombination.

In this theoretical background section, we have shown several points, where the 0D model has its limitations in the analysis of light-intensity-dependent J_{sc} -measurements. The J_{sc} – Φ relation shown in Equation (9) is implicitly relying on a spatially constant generation and recombination rate and charge-carrier densities throughout the solar cell and neglects space-charge effects. In order to study these assumptions and their limitations, we performed numerical drift-diffusion simulations of organic solar cells using the advanced semiconductor analysis (ASA) software.^[63] **Figure 1** shows the current–voltage characteristics at 1 sun of the solar cells modeled for this work. To first identify the impact of each recombination mechanism on the linearity of the short-circuit current density with illumination, we modeled a thin solar cell with an absorber thickness $d = 100$ nm and constant generation rate within the active layer. In this case, space-charge effects do not play an important role since the system is symmetric and the width of the space-charge region exceeds the active layer thickness. We implemented five types of recombination mechanisms including direct recombination, recombination via exponential band tails with Urbach energies E_U of 30, 55, and 80 meV and recombination via deep defect states. For de-

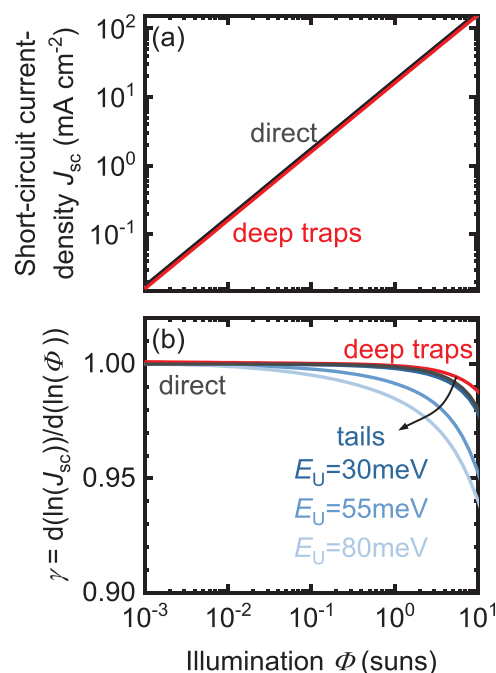


Figure 2. a) Light-intensity-dependent short-circuit current density J_{sc} of a solar cell with an active layer thickness $d = 100$ nm for direct recombination and trap-assisted recombination via trap states in the middle of the bandgap or tail states. b) Slope $\gamma = d(\ln(J_{sc}))/d(\ln(\Phi))$ for all three recombination mechanisms. In each case, J_{sc} deviates from a linear correlation with Φ at high light intensities with the strongest effect by exponential tail states with an Urbach energy $E_U = 80$ meV.

tailed simulation parameters we refer to **Table 1**. We chose the simulation parameters in a way that the power conversion efficiency under 1 sun illumination decreases from direct to deep-trap recombination (see **Figure 1a**). Thereby, we associate the efficiency under the influence of each recombination mechanism with the position of its trap states in the energy band. In a next step, we modeled a solar cell with $d = 300$ nm incorporating optical data for the contact layers (see **Figure S1**, Supporting Information) and simulated these under air mass (AM)1.5G spectrum to investigate the role of space charges on the light-intensity dependence of the short-circuit current density J_{sc} with different recombination mechanisms. **Figure 1b** displays the corresponding current–voltage characteristics under 1 sun.

3. Results

3.1. Thin Devices

In the following, we study an organic solar cell with constant generation throughout a thin active layer and discuss the different limitations of the 0D approximation that occur for each recombination mechanism.

Figure 2a shows the short-circuit current density J_{sc} as a function of illumination Φ for all recombination mechanisms. As J_{sc} does not differ strongly between the cells on a logarithmic scale, the curves nearly coincide and appear linear on this scale. Only looking at the derivative $\gamma = d(\ln(J_{sc}))/d(\ln(\Phi))$ as shown

Table 1. Simulation parameters for the solar cells modeled in ASA. The simulations for a thin device contain a variation of the generation rate that is constant throughout the active layer. The parameters adapted for a thick device are listed in brackets. For these simulations the generation rate is generated by ASA under AM1.5G spectrum and varied in intensity.

Parameter	Simulation with direct rec.	Simulation with rec. via tail states	Simulation with rec. via deep traps
Active layer thickness d [nm]	100 (300)	100 (300)	100 (300)
Effective density of states conduction band/valence band $N_{CB/VB}$ [cm ⁻³]	10^{19}	10^{19}	10^{19}
Energy gap E_{gap} [eV]	1.5	1.5	1.5
Injection barrier front/back contact $\phi_{bf/bb}$ [eV]	0.1	0.1	0.1
Electron/hole mobility $\mu_{e/h}$ [cm ² V ⁻¹ s ⁻¹]	10^{-4} (5×10^{-4})	10^{-4} (5×10^{-4})	10^{-4} (5×10^{-4})
Relative dielectric permittivity ϵ_r	3.8	3.8	3.8
Direct recombination coefficient k_{dir} [cm ³ s ⁻¹]	10^{-12}	–	–
Density of conduction/valence band tail states $N_{CBT/VBT}$ [cm ⁻³]	–	7.5×10^{17} (6×10^{17})	–
Urbach energy E_U [meV]	–	30/55/80	–
VBT hole/CBT electron capture coefficient β_1 [cm ³ s ⁻¹]	–	10^{-10}	–
VBT electron/CBT hole capture coefficient β_2 [cm ³ s ⁻¹]	–	10^{-12}	–
Energy level deep traps E_{dt} [eV]	–	–	0.75
Density of states deep traps N_{dt} [cm ⁻³]	–	–	7×10^{15} (5×10^{15})
Deep trap gaussian width ΔE_{dt} [eV]	–	–	0.1
Capture coefficient deep traps β_{dt} [cm ³ s ⁻¹]	–	–	10^{-10}

in Figure 2b reveals the different trends with illumination between the recombination mechanisms. In case of recombination via tail states, the slope differs from 1 at high light intensities. With increasing Urbach energy E_U , the degree of nonlinearity increases. In addition, the nonlinearity appears at lower light intensities in comparison to direct recombination. When treating tail state recombination as monomolecular recombination, this behavior contradicts the 0D model which supposes a linear correlation between the recombination and generation rate. According to our simulations, a highly linear J_{sc} – Φ relation rather indicates the absence of severe band tails. In contrast, J_{sc} mostly scales linearly with illumination up to one sun, when all recombination occurs via trap states in the middle of the bandgap as predicted by the rationale in Equation (9). A sublinear trend at low light intensities therefore suggests that recombination via deep traps is not the dominant recombination mechanism in a device. Yet, at light intensities above 1 sun, recombination via deep traps also causes a slope below unity in the $\log(J_{sc})$ – $\log(\Phi)$ plot. Hence, any kind of trap-assisted recombination can result in a sublinear trend, especially recombination via tail states, making it impossible to uniquely identify bimolecular recombination from J_{sc} – Φ measurements. This observation is further supported by the fact that J_{sc} of a solar cell with direct recombination does also not follow the trend predicted by Equation (9) but scales linearly with light intensity until high values, where it decreases.

Figure 3 explains this linear behavior of the J_{sc} for low light intensities that has been previously noted by Würfel et al.^[50] Figure 3a shows the electron densities n and the hole density p as a function of the position x in the active layer for different light intensities. In the center of the absorber layer, both charge-carrier densities scale with illumination Φ . At the contacts, however, only

the minority-charge carrier densities depend on Φ . As the recombination rate R scales with the product of both carrier concentrations, the correlation with light intensity changes within the active layer in Figure 3b. Under low illumination, the recombination rate near the contact is orders of magnitude higher than in the center. With increasing light intensity, the recombination in the middle becomes increasingly significant. Figure 3c shows the recombination rate R at the contact and in the middle of the active layer as a function of Φ . It has a slope of 2 in the center indicating a quadratic correlation since both electron density and hole density scale with illumination. At the contacts, the slope is 1 as only the minority-carrier concentration increases. The total recombination-current density $J_{rec,dir}(\Phi) = q \int_0^d R_{dir}(x, \Phi) dx$ follows the trend of the recombination at the contacts for low light intensities. As the recombination at the center of the active layer becomes more significant at high light intensities, $J_{rec,dir}$ increases more rapidly causing a nonlinear trend of the short-circuit current density J_{sc} with illumination Φ . With this approach, Würfel et al. demonstrated that a slope of 1 does not imply the absence of direct recombination.^[50] Yet, in their picture a slope below 1 is still a unique indicator for the process. With our simulations, we have shown that other recombination mechanisms can also exhibit sublinear behavior.

In the presence of Urbach tails in an organic solar cell, the nonlinearity of the short-circuit current density originates from a light-intensity dependence of the trapped charge-carrier densities. The density of states of exponential band tails is filled up to the quasi-Fermi level. Since the quasi-Fermi energy approaches the band edge with increasing light intensity, also an increasing number of trap states is occupied as illustrated in Figure 4a. The increase of the trapped charge-carrier density n_T with

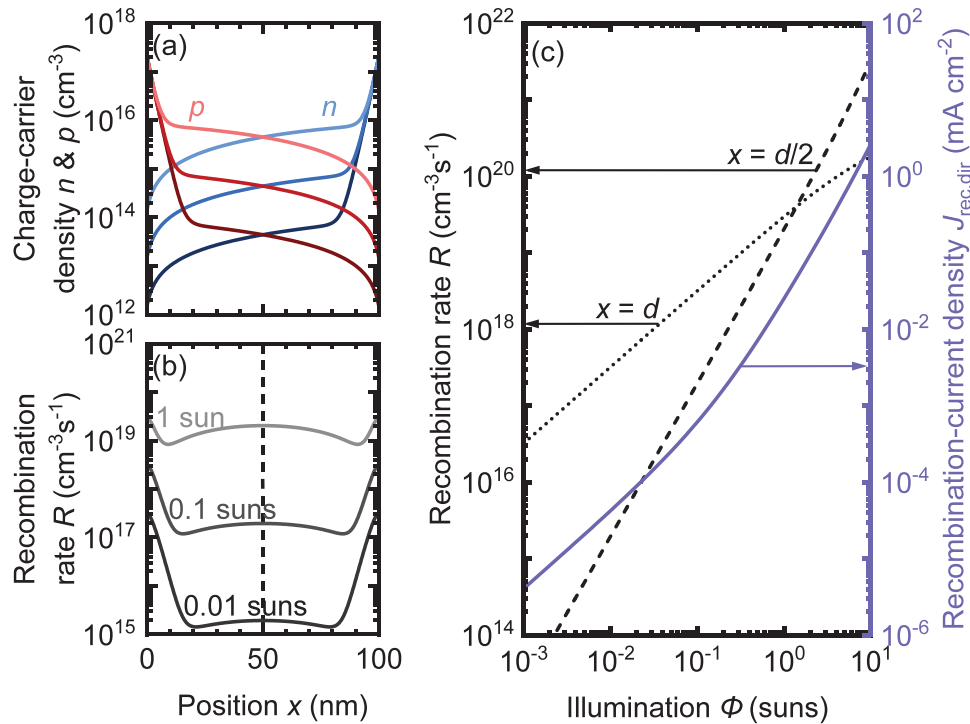


Figure 3. a) Charge-carrier density $n(x)$ and $p(x)$ of the electrons and holes, respectively, at different light intensities in a solar cell with direct recombination only. b) Recombination rate $R(x)$ for an illumination Φ of 0.01, 0.1, and 1 sun. c) Recombination rate R in the center ($x = d/2$) and at the contact ($x = d$) of the active layer and the total recombination-current density $J_{\text{rec,dir}}$ as a function of illumination Φ . For low light intensities, the recombination at the edges dominates where only the minority-charge carrier densities scale with illumination.

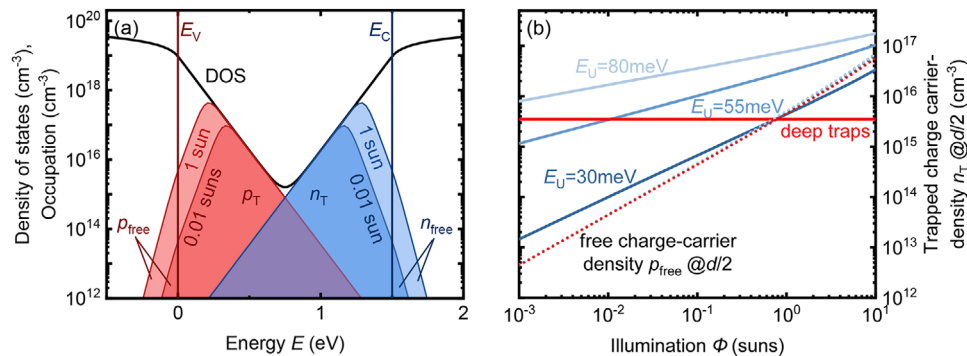


Figure 4. a) Energetic distribution of the density of states in a solar cell with exponential band tails and the occupation of these states at light intensities of 1 and 0.01 suns. The number of trapped charge carriers has its maximum at the quasi-Fermi level and therefore also changes with light intensity. b) Trapped electron density n_{T} as a function of illumination Φ for Urbach energies E_{U} of 30, 55, and 80 meV and trap states in the middle of the bandgap. Since the trapped carrier concentrations also increase with light intensity, the recombination with these charges is nonlinear.

illumination is also shown in Figure 4b for Urbach energies E_{U} of 30, 55, and 80 meV. As both free and trapped carrier densities increase with light intensity, the recombination rate scales superlinearly with Φ . In addition, we note that in Urbach tails with high values of E_{U} n_{T} increases less rapidly than for low E_{U} . Consequently, for solar cells with similar efficiency but different Urbach energies, the one with the lowest E_{U} shows the strongest sublinear trend in the $J_{\text{sc}}-\Phi$ relation (see Figure S2, Supporting Information). However, since we chose to have the highest power conversion efficiency under 1 sun illumination at $E_{\text{U}} = 30$ meV and the lowest at $E_{\text{U}} = 80$ meV for the simu-

lations, the correlation with E_{U} is opposite in Figure 2b due to a higher total recombination rate. Figure 4b also contains the trapped charge-carrier density of a solar cell with deep defects. In contrast to Urbach tails, the concentration of charges in deep traps remains unaffected by light intensity.

For deep defects, another limitation of the 0D model applies concerning the volume of the region that dominates the recombination rate. Figure 5a shows the carrier densities n and p for different positions x in the active layer and light intensities from 1 to 100 suns. Whereas the free charge-carrier densities increase with light intensity, the number of charges trapped in deep defect

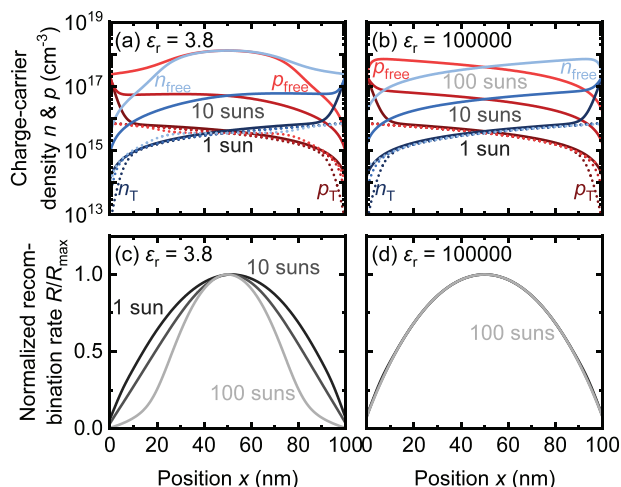


Figure 5. a,b) Electron density $n(x)$ and hole density $p(x)$ for light intensities of 1, 10, and 100 suns in a solar cell with recombination via deep traps for a realistic relative permittivity ϵ_r (a) and for a permittivity preventing space-charge effects (b). The free charge-carrier densities (solid lines) scale with illumination Φ whereas the trapped charge-carrier densities (dotted lines) remain mostly constant. c,d) Normalized recombination rate R/R_{\max} for increasing light intensities with $\epsilon_r = 3.8$ (c) and high ϵ_r (d). The width of the recombination rate decreases in a realistic cell causing nonlinearity the short-circuit current density J_{sc} due to space charges.

states remains constant in the middle of the absorber (compare Figure 4b). In addition, the total charge density ρ is decreasing with light intensity around the center as the free electron and hole density approach each other. Simultaneously, space charge near the contacts builds up. As a comparison, Figure 5b shows the charge-carrier densities for an infinitely high relative permittivity, guaranteeing a constant electric field throughout the solar cell. Indeed, it features more evenly distributed carrier densities. Also, it should be noted that the defect states implemented in these simulations are donor-like defects. Hence, when being occupied by a hole, they are positively charged. Therefore, an additional space charge occurs which is maximum at $x = 0$ nm. However, it is small in contrast to the symmetric space charge building up near both contacts. The effect of this space charge on the recombination rate can be depicted from Figure 5c,d. They show the normalized recombination rate R/R_{\max} for a solar cell with realistic permittivity and extremely high permittivity. In the presence of space charge, the shape of the recombination rate changes with light intensity whereas it remains the same under a constant electric field. In Figure 5c, the normalized recombination rate R/R_{\max} is maximum in the center but its width decreases with illumination. The normalized recombination rates for light intensities below 1 sun mostly coincide with the one at 1 sun and are therefore not shown in Figure 5c. The resulting recombination-current density $J_{\text{rec,SRH}}(\Phi) = q \int_0^d R_{\text{SRH}}(x, \Phi) dx \approx q d_{\text{eff}}(\Phi) \bar{R}_{\text{SRH}}(\Phi)$ thereby is not linear with illumination since the effective thickness d_{eff} , where the major part of the recombination occurs, changes with light intensity. This nonlinear recombination-current density translates to the short-circuit current density showing the influence of space charge even in thin devices.

Thereby, we have demonstrated that nonlinear recombination losses can occur for all recombination mechanisms caused by either a changing light-intensity dependence of charge-carrier densities at different positions in the active layer or by increasing numbers of carriers trapped in tail states. These effects violate the 0D approximation for thin active layers and constant generation. Even when the recombination mechanism itself is mostly linear, weak space-charge effects may even occur in thin devices. However, organic solar cell research aims at achieving higher active layer thicknesses for commercialization.^[14,64–66] In these layers, the generation rate can no longer be approximated as constant throughout the absorber and space-charge effects are increasingly significant. Therefore, we performed simulations implementing spatially dependent generation in solar cells with an absorber thickness $d = 300$ nm.

3.2. Thick Devices—The Role of Space Charge

In devices with a high absorber thickness, space-charge effects become increasingly significant as the layer thickness exceeds the width of the space-charge region. To illustrate the impact of different energetic distributions of defect states on the solar cell, Figure 6 shows the band diagrams under 1 sun illumination and the corresponding generation and recombination rates as a function of the position x . For direct recombination only, the field within the active layer in Figure 6a is mostly constant with only little band bending at the contacts. In the case of tail states, with increasing Urbach energies from Figure 6b–d, a low-field zone appears in the region, where generation and recombination are high in Figure 6g–i. As reported by Wu et al.,^[55] electrons are extracted at the illuminated contact whereas holes diffuse to the opposite contact. At the anode however, electrons are neither created in large amounts due to the position dependent generation rate nor can they diffuse from the cathode to the anode because of the opposing electric field. Therefore, a positive space charge builds up opposite to the illuminated contact causing a high-field and a low-field region.^[55,67] The diffusion-dominated low-field regime limits the short-circuit current density as most charge carriers recombine here (see Figure 6g–i). The band diagram in Figure 6e for a solar cell with recombination via deep traps also shows band bending similar to the case of $E_U = 30$ meV and thereby indicates that space-charge formation also matters for deep defects at light intensities around 1 sun.

Whereas the light-intensity dependence of space charge caused by asymmetric mobilities has already been analyzed by Wilken et al.,^[59] the influence on the J_{sc} – Φ relation of the space-charge region due to defect states as observed in Figure 6 still has to be investigated. For this purpose, Figure 7 shows the slope $\gamma = d(\ln(J_{sc}))/d(\ln(\Phi))$ as a function of illumination Φ . For a realistic device in Figure 7a, there is substantial nonlinearity occurring at lower light intensities than in Figure 7b for a device with high relative permittivity and therefore constant electric field. This observation indicates that space-charge effects are significant for each recombination mechanism investigated. A device with direct recombination also appears to be impacted by space-charge effects. At high light intensities, γ saturates to values close to $3/4$ as predicted by Equation (14) for the absence of defect states. For

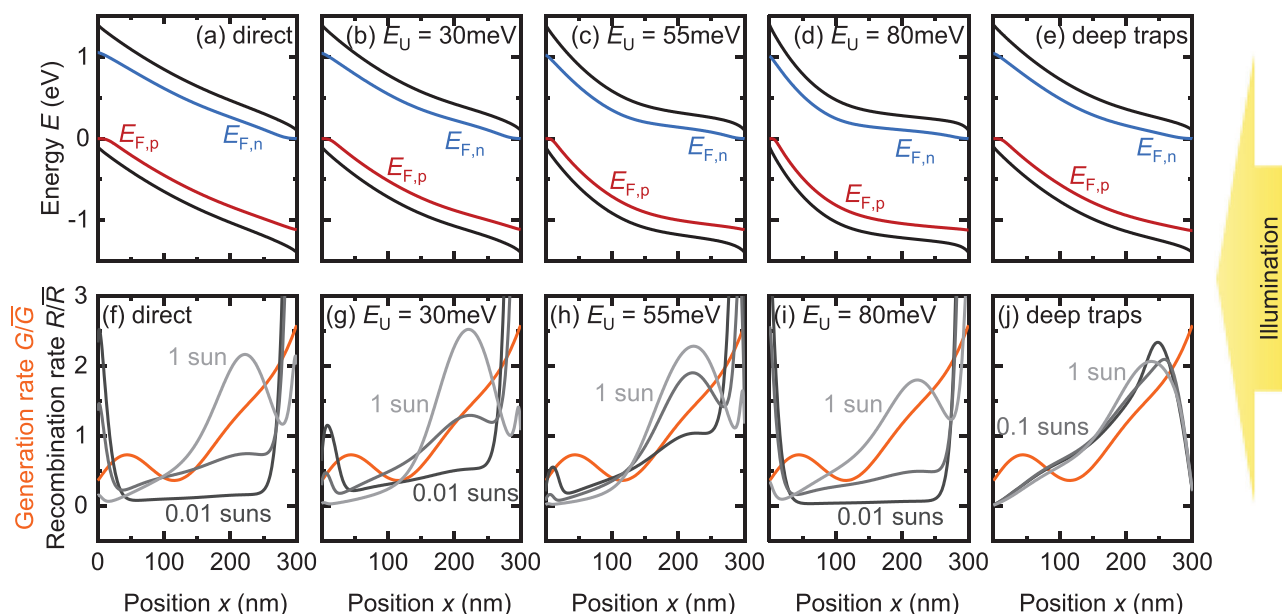


Figure 6. a–e) Band diagrams of solar cells with an active layer thickness $d = 300$ nm that are illuminated from the right with 1 sun illumination. f–j) Normalized generation rate G/\bar{G} and recombination rate R/\bar{R} as a function of position x in the active layer. Each simulation contains only one recombination mechanism, namely: a, f) direct recombination, a–d, g–i) recombination via tail states with increasing Urbach energy E_U , and e, j) recombination via deep traps. For more severe band tails, a low-field region forms where generation and recombination rates peak.

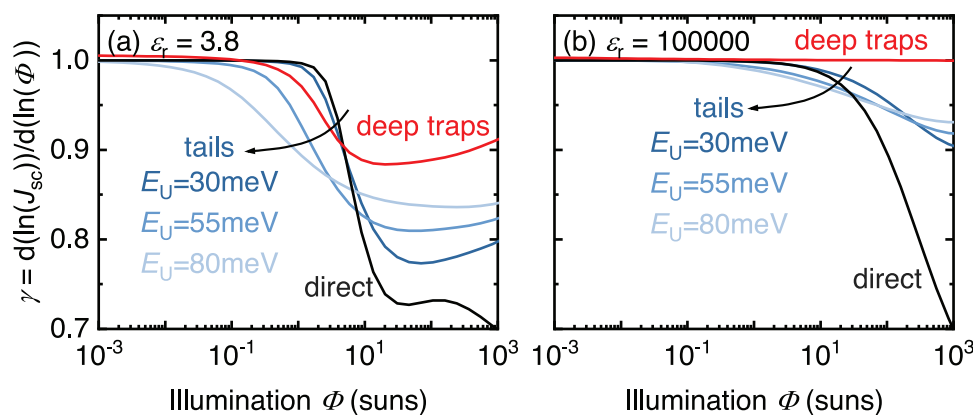


Figure 7. a, b) Slope $\gamma = d(\ln(J_{sc}))/d(\ln(\Phi))$ of the light-intensity-dependent short-circuit current density in a solar cell with an active layer thickness $d = 300$ nm and spatially dependent generation for different dominant charge-carrier recombination mechanisms. For a realistic relative permittivity $\epsilon_r = 3.8$ (a), nonlinear effects are more dominant than for a high permittivity (b) where the electric field is constant.

defect states in the form of exponential band tails, a strong non-linearity of J_{sc} can be observed at low light intensities already. The strongest impact can be seen for high Urbach energies E_U as these exhibit the most space charge. Thus, a highly linear J_{sc} – Φ relation indicates the absence of strong tail states as already observed for thin devices. However, the trend with E_U reverses under high illumination which is in line with Equation (17). The trend with E_U from our simulation coincides with the analytical solution for space-charge limited currents with tail states and contradicts the behavior that one might intuitively predict. When comparing Figure 7a,b, it occurs that next to direct and tail state recombination, a device with recombination via deep traps also exhibits strong space-charge effects. After showing a slope even

above 1 for low values of Φ , γ then falls below direct recombination around 1 sun and saturates to a relatively high value. The positive charge from holes in the donor-like defects further intensifies these space-charge effects since it is highest close to the anode. Acceptor-like defects would decrease the positive space charge. For the influence of the trap type on the J_{sc} – Φ relation, see Figure S3 in the Supporting Information. The same effect appears for actual doping. Unintentional doping has been observed in organic solar cells^[68–70] and is an additional source of space charge limiting the photocurrent and the performance.^[67,71,72] Deledalle et al. have previously demonstrated that p-type doping reduces the nonlinearity when the hole contact is illuminated.^[73] Here, n-type doping increases the space charge caused by the

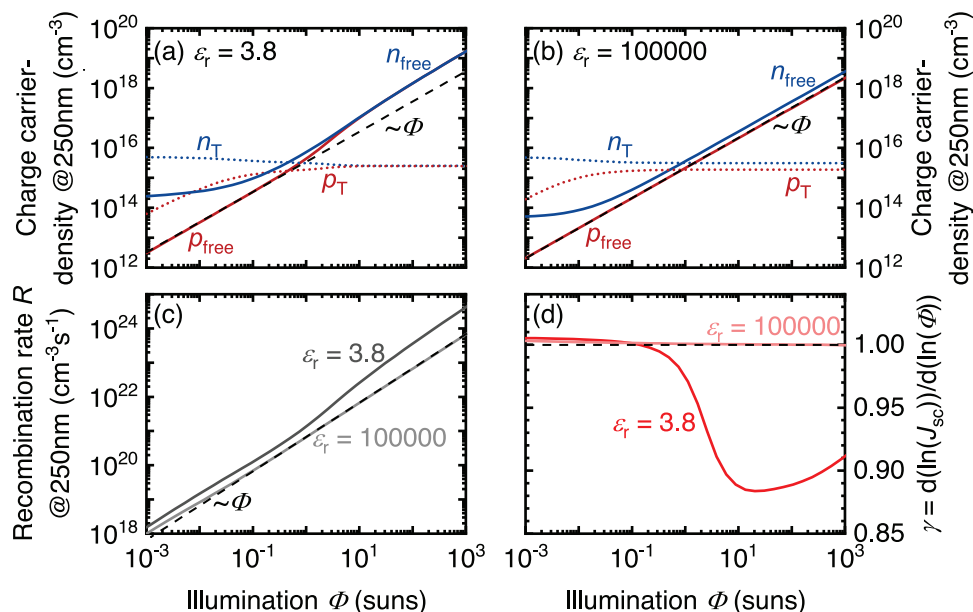


Figure 8. a) Free charge-carrier densities n_{free} and p_{free} of electrons and holes, respectively, and the trapped carrier densities n_{T} and p_{T} in defect states in the middle of the bandgap as a function of illumination Φ . A linear trend with Φ is indicated by the dashed line. b) Light-intensity dependence of the carrier densities in a solar cell with a high relative dielectric permittivity ϵ_r and therefore constant electric field. c) Recombination rate R at the position $x = 250$ nm in the active layer and d) slope $\gamma = d(\ln(J_{\text{sc}}))/d(\ln(\Phi))$ as a function of Φ for realistic and infinitely high ϵ_r . The nonlinearity of free charges and therefore R and γ under strong illumination only occurs for a realistic permittivity which highlights the role of space charge for solar cells with recombination via deep traps.

asymmetric illumination whereas p-type doping decreases it. The effect of doping on the light-intensity dependence of J_{sc} is illustrated in Figure S4 in the Supporting Information and coincides with the findings by Deledalle et al.

When comparing the recombination mechanisms, most strikingly, direct recombination features the least sublinearity up to light intensities above 1 sun out of all recombination parameters chosen. This observation opposes the conventional approaches to the relation between the short-circuit current density and the illumination displayed in Figure 7a. For the correct interpretation, neither the 0D model nor the consideration of space charges with a $J_{\text{sc}} \sim G^{3/4}$ relation is sufficient. Instead, our application of the Mark–Helfrich equation to a diode is required to explain the tail states' impact. The space-charge effects in the presence of deep defects require even further examination.

For this purpose, **Figure 8** shows the charge-carrier densities around the maximum of the recombination rate R at $x = 250$ nm. In Figure 8a, the free hole density p_{free} increases linearly with light intensity first and then more rapidly under higher illumination. The free electron density n_{free} only increases slowly with light intensity for low values of Φ and follows p_{free} for high values. Also, the trapped carrier densities are not constant but the electron concentration n_{T} decrease and consequently, the holes density p_{T} increase with Φ . To identify nonlinearity caused by space-charge effects, Figure 8b shows the charge-carrier densities for a high relative permittivity ϵ_r and therefore for a constant electric field. Indeed, in the illumination range around 1 sun, the trapped charge-carrier densities remain constant and both n_{free} and p_{free} increase linearly with light intensity causing a linear trend in the recombination rate R in Figure 8c. The superlinear behavior of R evoked by space charges yields a slope $\gamma = d(\ln(J_{\text{sc}}))/d(\ln(\Phi))$ in

Figure 8d that drops below 1 for a realistic relative permittivity ϵ_r around 1 sun already.

Another effect can be observed at low illumination. Here, the charges that recombine with each other have to be examined in pairs since the recombination rate scales with the product of n_{free} and p_{T} as well as p_{free} and n_{T} . The trapped electron density n_{T} decreases while p_{free} increases linearly causing the product $p_{\text{free}} \times n_{\text{T}}$ to have a slope below 1. The product $n_{\text{free}} \times p_{\text{T}}$ features the same trend resulting in the recombination rate R to increase only slowly in Figure 8c. This sublinear recombination rate yields values higher than 1 for $\gamma = d(\ln(J_{\text{sc}}))/d(\ln(\Phi))$ in Figure 8d. Therefore, the light-intensity dependence of the short-circuit current density in the presence of deep trapping states can be explained by a sublinear recombination rate under low illumination and space charges at high light intensities.

In the results presented above on solar cells with thick active layers, we have shown that space charges can build up for each recombination mechanism under high illumination, causing an even more drastic nonlinearity of the $J_{\text{sc}}-\Phi$ relation than the effects discussed for thin devices. These sublinear trends cannot be explained by the model previously used for space-charge limited photocurrent but require the consideration of trap states.

4. Conclusion

In this work, we presented a detailed discussion on the light-intensity dependence of the short-circuit current density J_{sc} which is a method widely used to identify bimolecular recombination in organic solar cells.^[29–37] The simplicity of the method is based on a number of assumptions including the neglect of any

spatial dependence of the generation and recombination rate and of space charges. Picking up on the findings by Würfel et al.,^[50] that bimolecular recombination scales linearly with illumination Φ , when recombination at the contacts dominates, we examined other recombination mechanisms. With our simulations, we have shown that devices with trap-assisted recombination exhibit a sublinear J_{sc} – Φ relation that might be falsely identified as bimolecular recombination by this method. Recombination via tail states features a sublinear trend due to the light-intensity dependence of the trapped carrier concentrations. In the presence of trap states in the middle of the energy gap, the spatial resolution of the recombination rate R gains importance as the volume with significant recombination changes with illumination Φ . The effect is evoked by space charges but remains small for thin devices. We have further discussed the increasing impact of charged trap states on the J_{sc} – Φ relation under nonuniform generation in thick devices which cannot be explained by the conventional model for space-charge limited photocurrent in diodes.

Thereby, our simulations deliver a better understanding of the influence of different recombination mechanisms on the J_{sc} – Φ relation that allows analyzing experimental data accordingly. A sublinear trend measured in thin devices at low light intensities rules out recombination via deep traps as dominant recombination mechanisms. In contrast, a highly linear correlation might still include direct and deep trap recombination but not major losses via tail states independent of the absorber thickness. Instead, strong band tails are indicated by sublinear behavior at low light intensities in thick devices. Therefore, our work offers a new approach to interpreting J_{sc} – Φ measurements considering several recombination mechanisms and active layer thicknesses.

Supporting Information

Supporting Information is available from the Wiley Online Library or from the author.

Acknowledgements

T.K. and P.H. acknowledge funding by the Helmholtz Association.
Open access funding enabled and organized by Projekt DEAL.

Conflict of Interest

The authors declare no conflict of interest.

Keywords

absorber thickness, deep defects, recombination, space charge, tail states

Received: May 21, 2020
Revised: July 10, 2020
Published online: August 18, 2020

- [1] H. Li, Z. Xiao, L. Ding, J. Wang, *Sci. Bull.* **2018**, 63, 340.
- [2] X. Song, N. Gasparini, L. Ye, H. Yao, J. Hou, H. Ade, D. Baran, *ACS Energy Lett.* **2018**, 3, 669.

- [3] X. Che, Y. Li, Y. Qu, S. R. Forrest, *Nat. Energy* **2018**, 3, 422.
- [4] D. Baran, N. Gasparini, A. Wadsworth, C. H. Tan, N. Wehbe, X. Song, Z. Hamid, W. Zhang, M. Neophytou, T. Kirchartz, C. J. Brabec, J. R. Durrant, I. McCulloch, *Nat. Commun.* **2018**, 9, 2059.
- [5] Y. Cui, H. Yao, J. Zhang, T. Zhang, Y. Wang, L. Hong, K. Xian, B. Xu, S. Zhang, J. Peng, Z. Wei, F. Gao, J. Hou, *Nat. Commun.* **2019**, 10, 2515.
- [6] J. Yuan, Y. Zhang, L. Zhou, G. Zhang, H.-L. Yip, T.-K. Lau, X. Lu, C. Zhu, H. Peng, P. A. Johnson, M. Leclerc, Y. Cao, J. Ulanski, Y. Li, Y. Zou, *Joule* **2019**, 3, 1140.
- [7] Y. Cui, H. Yao, J. Zhang, K. Xian, T. Zhang, L. Hong, Y. Wang, Y. Xu, K. Ma, C. An, *Adv. Mater.* **2020**, 10, 2515.
- [8] R. Ma, T. Liu, Z. Luo, Q. Guo, Y. Xiao, Y. Chen, X. Li, S. Luo, X. Lu, M. Zhang, *Sci. China: Chem.* **2020**, 63, 325.
- [9] X. Du, Y. Yuan, L. Zhou, H. Lin, C. Zheng, J. Luo, Z. Chen, S. Tao, L. S. Liao, *Adv. Funct. Mater.* **2020**, 30, 1909837.
- [10] L. Zhan, S. Li, T.-K. Lau, Y. Cui, X. Lu, M. Shi, C.-Z. Li, H. Li, J. Hou, H. Chen, *Energy Environ. Sci.* **2020**, 13, 635.
- [11] Q. Liu, Y. Jiang, K. Jin, J. Qin, J. Xu, W. Li, J. Xiong, J. Liu, Z. Xiao, K. Sun, *Sci. Bull.* **2020**, 65, 272.
- [12] D. Baran, T. Kirchartz, S. Wheeler, S. Dimitrov, M. Abdelsamie, J. Gorman, R. S. Ashraf, S. Holliday, A. Wadsworth, N. Gasparini, P. Kaienburg, H. Yan, A. Amassian, C. J. Brabec, J. R. Durrant, I. McCulloch, *Energy Environ. Sci.* **2016**, 9, 3783.
- [13] P. Cheng, M. Zhang, T. K. Lau, Y. Wu, B. Jia, J. Wang, C. Yan, M. Qin, X. Lu, X. Zhan, *Adv. Mater.* **2017**, 29, 1605216.
- [14] J. Gao, W. Gao, X. Ma, Z. Hu, C. Xu, X. Wang, Q. An, C. Yang, X. Zhang, F. Zhang, *Energy Environ. Sci.* **2020**, 13, 958.
- [15] J.-L. Wang, K.-K. Liu, L. Hong, G.-Y. Ge, C. Zhang, J. Hou, *ACS Energy Lett.* **2018**, 3, 2967.
- [16] Z. Luo, C. Sun, S. Chen, Z.-G. Zhang, K. Wu, B. Qiu, C. Yang, Y. Li, C. Yang, *Adv. Energy Mater.* **2018**, 8, 1800856.
- [17] J. Benduhn, K. Tvingstedt, F. Piersimoni, S. Ullbrich, Y. Fan, M. Tropicano, K. A. McGarry, O. Zeika, M. K. Riede, C. J. Douglas, S. Barlow, S. R. Marder, D. Neher, D. Spoltore, K. Vandewal, *Nat. Energy* **2017**, 2, 17053.
- [18] M. Azzouzi, J. Yan, T. Kirchartz, K. Liu, J. Wang, H. Wu, J. Nelson, *Phys. Rev. X* **2018**, 8, 031055.
- [19] F. D. Eisner, M. Azzouzi, Z. Fei, X. Hou, T. D. Anthopoulos, T. J. S. Dennis, M. Heeney, J. Nelson, *J. Am. Chem. Soc.* **2019**, 141, 6362.
- [20] S. Ullbrich, J. Benduhn, X. Jia, V. C. Nikolis, K. Tvingstedt, F. Piersimoni, S. Roland, Y. Liu, J. Wu, A. Fischer, D. Neher, S. Reineke, D. Spoltore, K. Vandewal, *Nat. Mater.* **2019**, 18, 459.
- [21] K. Huang, A. Rhys, *Proc. R. Soc. London, Ser. A* **1950**, 204, 406.
- [22] B. K. Ridley, *Solid-State Electron.* **1978**, 21, 1319.
- [23] B. K. Ridley, *J. Phys. C: Solid State Phys.* **1978**, 11, 2323.
- [24] T. Markvart, *J. Phys. C: Solid State Phys.* **1981**, 14, L895.
- [25] T. Markvart, in *Recombination in Semiconductors*, (Eds: P. T. Landsberg), Cambridge University Press, Cambridge **2003**.
- [26] T. Kirchartz, T. Markvart, U. Rau, D. A. Egger, *J. Phys. Chem. Lett.* **2018**, 9, 939.
- [27] G. F. A. Dibb, T. Kirchartz, D. Credgington, J. R. Durrant, J. Nelson, *J. Phys. Chem. Lett.* **2011**, 2, 2407.
- [28] D. Credgington, J. R. Durrant, *J. Phys. Chem. Lett.* **2012**, 3, 1465.
- [29] L. J. A. Koster, V. D. Mihailetchi, H. Xie, P. W. M. Blom, *Appl. Phys. Lett.* **2005**, 87, 203502.
- [30] L. J. A. Koster, M. Kemerink, M. M. Wienk, K. Maturova, A. J. Janssen, *Adv. Mater.* **2011**, 23, 1670.
- [31] C. Sun, F. Pan, H. Bin, J. Zhang, L. Xue, B. Qiu, Z. Wei, Z. G. Zhang, Y. Li, *Nat. Commun.* **2018**, 9, 743.
- [32] B. Guo, W. Li, X. Guo, X. Meng, W. Ma, M. Zhang, Y. Li, *Adv. Mater.* **2017**, 29, 1702291.
- [33] G. Zhang, G. Yang, H. Yan, J. H. Kim, H. Ade, W. Wu, X. Xu, Y. Duan, Q. Peng, *Adv. Mater.* **2017**, 29, 1606054.
- [34] L. Yang, S. Zhang, C. He, J. Zhang, H. Yao, Y. Yang, Y. Zhang, W. Zhao, J. Hou, *J. Am. Chem. Soc.* **2017**, 139, 1958.

- [35] Y. Lin, F. Zhao, Y. Wu, K. Chen, Y. Xia, G. Li, S. K. K. Prasad, J. Zhu, L. Huo, H. Bin, Z. G. Zhang, X. Guo, M. Zhang, Y. Sun, F. Gao, Z. Wei, W. Ma, C. Wang, J. Hodgkiss, Z. Bo, O. Inganas, Y. Li, X. Zhan, *Adv. Mater.* **2017**, 29, 1604155.
- [36] S. R. Cowan, A. Roy, A. J. Heeger, *Phys. Rev. B* **2010**, 82, 245207.
- [37] F. Zhao, S. Dai, Y. Wu, Q. Zhang, J. Wang, L. Jiang, Q. Ling, Z. Wei, W. Ma, W. You, C. Wang, X. Zhan, *Adv. Mater.* **2017**, 29, 1700144.
- [38] C. Deibel, A. Wagenpfahl, *Phys. Rev. B* **2010**, 82, 207301.
- [39] C. M. Amb, M. R. Craig, U. Koldemir, J. Subbiah, K. R. Choudhury, S. A. Gevorgyan, M. Jørgensen, F. C. Krebs, F. So, J. R. Reynolds, *ACS Appl. Mater. Interfaces* **2012**, 4, 1847.
- [40] A. Armin, M. Hamsch, P. Wolfers, H. Jin, J. Li, Z. Shi, P. L. Burn, P. Meredith, *Adv. Energy Mater.* **2015**, 5, 1401221.
- [41] T. Wang, X.-Y. Yang, P.-Q. Bi, M.-S. Niu, L. Feng, J.-Q. Liu, X.-T. Hao, *Sol. RRL* **2019**, 3, 1900087.
- [42] J. Zhang, Y. Zhao, J. Fang, L. Yuan, B. Xia, G. Wang, Z. Wang, Y. Zhang, W. Ma, W. Yan, W. Su, Z. Wei, *Small* **2017**, 13, 1700388.
- [43] G. Zhang, K. Zhang, Q. Yin, X.-F. Jiang, Z. Wang, J. Xin, W. Ma, H. Yan, F. Huang, Y. Cao, *J. Am. Chem. Soc.* **2017**, 139, 2387.
- [44] A. M. Goodman, A. Rose, *J. Appl. Phys.* **1971**, 42, 2823.
- [45] V. D. Mihailetschi, J. Wildeman, P. W. M. Blom, *Phys. Rev. Lett.* **2005**, 94, 126602.
- [46] R. A. Street, D. M. Davies, *Appl. Phys. Lett.* **2013**, 102, 043305.
- [47] L. N. S. Murthy, D. Barrera, L. Xu, A. Gadh, F.-Y. Cao, C.-C. Tseng, Y.-J. Cheng, J. W. P. Hsu, *J. Phys. Chem. C* **2019**, 123, 10795.
- [48] R. A. Street, A. Krakaris, S. R. Cowan, *Adv. Funct. Mater.* **2012**, 22, 4608.
- [49] C. G. Shuttle, N. D. Treat, J. D. Douglas, J. M. J. Fréchet, M. L. Chabinyc, *Adv. Energy Mater.* **2012**, 2, 111.
- [50] U. Würfel, L. Perdigón-Toro, J. Kurpiers, C. M. Wolff, P. Caprioglio, J. Rech, J. Zhu, X. Zhan, W. You, S. Shoaee, D. Neher, M. Stollerfoht, *J. Phys. Chem. Lett.* **2019**, 10, 3473.
- [51] G. Lakhwani, A. Rao, R. H. Friend, *Annu. Rev. Phys. Chem.* **2014**, 65, 557.
- [52] C. Göhler, A. Wagenpfahl, C. Deibel, *Adv. Electron. Mater.* **2018**, 4, 1700505.
- [53] S. A. Hawks, G. Li, Y. Yang, R. A. Street, *J. Appl. Phys.* **2014**, 116, 074503.
- [54] R. Street, *Phys. Rev. B* **2011**, 84, 075208.
- [55] J. Wu, J. Luke, H. K. H. Lee, P. Shakya Tuladhar, H. Cha, S.-Y. Jang, W. C. Tsoi, M. Heeney, H. Kang, K. Lee, T. Kirchartz, J.-S. Kim, J. R. Durrant, *Nat. Commun.* **2019**, 10, 5159.
- [56] S. Liu, J. Yuan, W. Deng, M. Luo, Y. Xie, Q. Liang, Y. Zou, Z. He, H. Wu, Y. Cao, *Nat. Photonics* **2020**, 14, 300.
- [57] R. S. Crandall, Q. Wang, E. A. Schiff, in *Conference Record of the Twenty Fifth IEEE Photovoltaic Specialists Conference-1996*, IEEE, New York **1996**, p. 1113.
- [58] N. F. Mott, R. W. Gurney, *Electronic Processes in Ionic Crystals*, Oxford University Press, New York **1948**.
- [59] S. Wilken, O. J. Sandberg, D. Scheunemann, R. Österbacka, *Sol. RRL* **2020**, 4, 1900505.
- [60] J. A. Röhr, D. Moia, S. A. Haque, T. Kirchartz, J. Nelson, *J. Phys.: Condens. Matter* **2018**, 30, 105901.
- [61] P. Mark, W. Helfrich, *J. Appl. Phys.* **1962**, 33, 205.
- [62] T. Kirchartz, *Beilstein J. Nanotechnol.* **2013**, 4, 180.
- [63] M. Zeman, J. Krc, *J. Mater. Res.* **2008**, 23, 889.
- [64] Y. Zhang, H. Feng, L. Meng, Y. Wang, M. Chang, S. Li, Z. Guo, C. Li, N. Zheng, Z. Xie, *Adv. Energy Mater.* **2019**, 9, 1902688.
- [65] L. Ma, Y. Xu, Y. Zu, Q. Liao, B. Xu, C. An, S. Zhang, J. Hou, *Sci. China: Chem.* **2020**, 63, 21.
- [66] L. Ma, S. Zhang, H. Yao, Y. Xu, J. Wang, Y. Zu, J. Hou, *ACS Appl. Mater. Interfaces* **2020**, 12, 18777.
- [67] T. Kirchartz, T. Agostinelli, M. Campoy-Quiles, W. Gong, J. Nelson, *J. Phys. Chem. Lett.* **2012**, 3, 3470.
- [68] O. J. Sandberg, M. Nyman, R. Österbacka, *Org. Electron.* **2014**, 15, 3413.
- [69] M. Nyman, O. J. Sandberg, S. Dahlström, D. Spoltore, C. Körner, Y. Zhang, S. Barlow, S. R. Marder, K. Leo, K. Vandewal, R. Österbacka, *Sci. Rep.* **2017**, 7, 5397.
- [70] M. Nyman, S. Dahlström, O. J. Sandberg, R. Österbacka, *Adv. Energy Mater.* **2016**, 6, 1600670.
- [71] V. A. Trukhanov, V. V. Bruevich, D. Y. Paraschuk, *Phys. Rev. B* **2011**, 84, 205318.
- [72] G. F. A. Dibb, M.-A. Muth, T. Kirchartz, S. Engmann, H. Hoppe, G. Gobsch, M. Thelakkat, N. Blouin, S. Tierney, M. Carrasco-Orozco, J. R. Durrant, J. Nelson, *Sci. Rep.* **2013**, 3, 3335.
- [73] F. Deledalle, T. Kirchartz, M. S. Vezie, M. Campoy-Quiles, P. Shakya Tuladhar, J. Nelson, J. R. Durrant, *Phys. Rev. X* **2015**, 5, 011032.